Electrical Tuning of Surface Plasmon Polariton Propagation in Graphene-Nanowire Hybrid Structure

Haoliang Qian,[1, +] Yaoguang Ma,[3, +] Qing Yang[1, +, *], Bigeng Chen,[1] Ying Liu,[2] Xin Guo,[1] Shisheng Lin,[4] Jili Ruan,[1] Xu Liu,[1]Limin Tong,[1] and Zhong Lin Wang[2, 5, *]

[1]State Key Laboratory of Modern Optical Instrumentation, Department of Optical Engineering, Zhejiang University, Hangzhou 310027, P.R. China

[2]School of Material Science and Engineering, Georgia Institute of Technology, Atlanta, Georgia, 30332-0245, United States

[3]State Key Laboratory for Mesoscopic Physics and Department of Physics, Peking University, Beijing 100871, P.R. China

[4]Department of Information Science and Electronic Engineering, Zhejiang University, Hangzhou 310027, P.R. China

[5] Satellite Research Facility, MANA, International Center for Materials Nanoarchitectonics, National Institute for Materials Science, 1-1 Namiki, Tsukuba, 305-0044, Japan

[+]These authors contributed equally in this work

[*] qingyang@zju.edu.cn; zhong.wang@mse.gatech.edu

We demonstrate a dynamic surface plasmonic modulation of graphene-nanowire hybrid structures in visible light range, which was thought to be a tough task for graphene based field effect transistor modulator previously. Static modulation depth of as high as 0.07 dB/μm has been achieved experimentally. Carefully simulation indicates the strongly focused electromagnetic field and dramatically enhanced electric field at the interface between a silver NW and a graphene sheet are key roles for bringing the optical response of the device to the visible range. Furthermore, the modulation behaviors near the Dirac point of monolayer graphene and the singularity of gap-induced bilayer graphene are investigated.

A surface plasmon polariton (SPP) is an electromagnetic excitation existing and propagating at the interface between a dielectric and a metal. SPPs can be both generated by an irradiating electromagnetic wave with high energy resolution [1-8] or high energy electrons with extremely high spatial resolution [9-11]. Due to the ability to produce highly enhanced optical fields below the diffraction limit [1, 2], SPP has wide scientific and technological applications such as SPP lasers [3, 4], optical antennas [5, 6], optical sensors [7] and subwavelength waveguides [8]. It is desired to have the ability to dynamically manipulate SPPs for their practical applications in modern information and communication technologies, preferably by applying an electrical bias. However, even noble metals, which are widely regarded as the best candidate for plasmonic materials, are hardly tunable simply through the electrical operation partially because of the difficulties in changing the carrier density [12,13]. On the other hand, graphene, a two dimensional sheet of carbon atoms, has shown large potential in achieving electrical control of

light, due to its fast carrier velocity and the low carrier scattering rate at room temperature [13-15]. In the past few years, graphene-based infrared and terahertz modulators have been reported by controlling the electronic structure of graphene [16-22]. Most recently, electrical controlled plasmonic scattering resonance has been demonstrated using the hybrid graphene/metal-nanostructure [23-25]. Active tunability of plasmonics transmission has also been achieved by coupling plasmons to optically active materials [26, 27]. To our best knowledge, there are few reports on electrical tuning of optical frequency (including visible to near-infrared) SPPs transmission using field effect transistor (FET) structure, because of the extreme challenge due to weak free electron responses, huge transmission losses in this spectra range and the limited carrier concentration achieved before the breakdown of the insulator layer in FET structure.

Here we report electric tuning of plasmonic behavior in a graphene-nanowire (graphene-NW) hybrid structure, in which the modulation is achieved through effectively tuning the Fermi level (E_f) of graphene by an externally applied gate voltage. Careful simulation indicates the charge distribution in the graphene is altered by the silver nanowire, which makes the charge density much higher around the vicinity of the nanowire approaching $0.921\times10^{14}cm^{-2}$. It was thought to be a tough task for graphene based FET modulator and only be achieved by high capacitance ion gel previously [28, 29]. We also compare the electrical controlling properties of SPPs based on monolayer and bilayer graphene, especially investigate the modulation behavior near the Dirac point of monolayer graphene and the singularity of gap-induced bilayer graphene. The theoretical calculation using the local random phase approximation (RPA) and the tight-binding model shows excellent agreement with experimental results.

Figure 1a shows schematic diagram of our device structure. A single layer of graphene fabricated using exfoliation method [30] is first transferred onto the top of a 300-nm-thick SiO_2 layer of a silicon wafer. The graphene is slightly p-doped because of the exposure to oxygen and moisture during the fabrication process of the device [31]. Then the silicon layer and the graphene sheet are connected to a picoammeter (KEITHLEY 6487) for applying bias voltage and electrical measurement. A 500-nm-diameter silver NW is finally placed on the graphene sheet, with its launching port placed outside the graphene sheet to ensure that the coupling efficiency will not be affected by the variation of the absorption of graphene under modulation [middle inset of Fig. 1(a)]. It is possible that silver NW may have direct carrier transferring into graphene considering their work function. In our experiments, the silver NW and graphene are physically contacted. According to the density function theory [32], the carrier transferring between the silver NW and graphene will pull down the Fermi level of the naturally p-doped graphene and keep it p-doped. Thus, the carrier transfer will not vary the doping condition and could be neglected in analyzing and simulation. A 659-nm-wavelength laser is used to excite SPPs in silver NWs on the graphene sheet through a $100\times$ high numerical aperture (NA=0.9) objective [Supplemental Material [33], Fig. S1]. The focused light is scattered into guided modes transmitted by the silver NW as SPPs [upper right inset of Fig. 1(a)]. The output light is detected by a CCD located on top of the structure. The measured stability of the system shows the time dependent fluctuation of the laser intensity used in the experiments is less than 1% [Supplemental Material [33], Fig. S2]. The monolayer graphene is confirmed by Raman spectroscopy (532-nm-wavelength laser pumping) from the G-peak and 2D-peak features in Fig. 1(b) [34, 35].

Figure 2 displays the static electro-optical response of the device characterized under

different driven voltages, V_D, when a 659-nm-wavelength light is transmitted through. The experimental data are normalized to the transmissivity value at zero bias voltage. The optical absorption of graphene is determined by the position of the Fermi level through Pauli Blocking effects, since interband transitions occurs when electrons are excited by the incoming photons ($h\nu$). And the graphene Fermi level can be tuned by applying a driving voltage on it, thus the total transmission can be modulated electrically. With the current structure design, the modulation depth, which is the logarithm of the ratio of the output light normalized to the NW length under bias voltage to its unbiased level, is as high as 0.07 dB/μm. The total modulation depth of our modulator will reach 3 dB if the interaction distance exceeds 40 μm. Additionally, comparison experiments are carried out on a SiO_2-Si structure without graphene and SiO_2-Si structure with gold film instead of graphene. No electrical modulation is achieved under the same measurement conditions, which indicates that graphene plays an important role in the modulation process [Supplemental Material [33], Fig. S3].

Carefully analyzing the static electro-optical response of the device, we find that the response curve can be divided into three parts, region I, II and III, respectively. When the device is driven with large positive bias voltage (region I, V_D>20 V, the graphene sheet is injected with abundance holes), a sharp increase of the transmission is observed. In this range, the Fermi level is pulled down. Because the occupation density decreases sharply above the Fermi level [14], when the Fermi level is lower than half of the photon energy, there will be hardly any electron transition due to photon excitation, thus the absorption of the graphene will be decreased and the SPP transmission will be increased. When the device is driven at large negative voltage (region III, V_D< -30V, the graphene sheet is injected with abundance electrons), the Fermi level surpasses the Dirac point. And when it is higher than half of the photon energy, all electron states interacting with incident photons will be occupied. Owing to the conservation of momentum and limited phonon energy, the newly occupied electrons at high levels of the linear band cannot be excited to even higher levels. Thus, the graphene appears transparent. Theoretically, a sharp increase of transmission should be observed at Fermi level $E_f = \pm h\nu/2$. However, in reality, defects in the graphene and natural doping will make the transition broaden and shift to higher voltage [19]. When the device is driven under low driving voltages (region II, -30 V < V_D < 20 V), the absolute value of the Fermi level is lower than half of the photon energy and interband transition occurs. According to previous reports [19], the optical transition in this range is insensitive to the driven voltage V_D. However, in experiments, we find the transmissivity depends on V_D and there is a minimum value near the Dirac point. In order to understand the modulation behavior in range II, we calculate the absorbance A near the Dirac point using the optical conductivity of graphene as a function of Fermi level E_f [36-38] [see Supplemental Material [33], section 5] and plot the curve for normalized transmissivity $10*\log((1-A)/(1-A_0))$ for different wavelengths in Fig. 2(b), where A and A_0 represent the absorption under the driving voltage and E_f=0 eV. In this plot, the Fermi level, expressed in unit of eV, can be regarded as a characterization of the driving voltage. It can be seen that the minimum transmissivity occurs at E_f = 0 eV. Therefore, there may exist a transmissivity valley near the Dirac point. The calculation also predicts that this transmission decrease will be more obvious in the infrared range.

It is noting that pushing the Fermi level of graphene to visible range is a very tough task for FET-like structures and it can only be achieved by liquid ion gel by utilizing its extremely high

capacitance density so far [28, 29]. The charge accumulated at about 20-30 V using a 300 nm SiO_2 as dielectric layer is not sufficient to shift the Fermi level enough for 659-nm-wavelength light according to the intuition expression [19]. However, the structure used in our experiments is fundamentally different from previous works [19]. Theoretical simulation shows the introduction of Ag NW on graphene will confine the light strongly at the interface and alter the charge distribution in graphene simultaneously. From the simulation shown in Fig. 3, we see that the electromagnetic energy is concentrated at the interface of the Ag NW and the graphene sheet, so that shifting the Femi level of graphene will greatly affect the interaction between graphene and SPPs through Pauli Blocking [39]. Besides the light confinement effect, electric field confinement effect under the Ag NW is very important for bringing the optical response of the device to the visible range. The simulation in Fig. 4 indicates the charge density around the vicinity of the NW is much higher than other areas (about two orders of magnitude/total effective area) due to different material properties of graphene and silver. We can use the equation $2E_f = 2\hbar v_f \sqrt{\eta\pi |\mathrm{V}+\mathrm{V}_0|} = 2\hbar v_f \sqrt{n\pi}$ [19, 29] to approximately estimate the Fermi level and the applied voltages. v_f is the Fermi velocity, V is the applied voltage, and V_0 is the voltage offset caused by the natural doping. And $n = \eta|V+V_0| = C|V+V_0|/e$, represents carrier concentration, where C is the effective capacitance density. The dual-confinement effect of charge density and electromagnetic energy around the vicinity of the NW will dramatic enhanced the light-matter interaction and increase the Fermi level shifting. Through calculation and comparison, we estimated the η could be at least $2.63\times10^{16} m^{-2}V^{-1}$ and n reaches $0.921\times10^{14} cm^{-2}$ after applying more than 25 V voltages, which is enough to shift the Fermi level for visible light [see Supplemental Material [33], section 6]

Additionally, we compare the modulation behavior of bilayer and monolayer graphene. Figure 5(a) shows the modulation experiments based on a bilayer graphene. We identify the number of the layers of graphene by Raman spectroscopy (using 532-nm-wavelength laser pumping) [34, 35], as displayed in Fig. 5(b). The bilayer graphene still have the absorption tunability, and the trend at large negative (region IV) and positive voltage (region I) is similar to the monolayer's. However, some highly repeatable difference exists at low driving voltage. There are two minimum value rather than one minimum value near E_f=0 eV (region II and III). The two transmissivity valley may be attributed to the bandgap induced by the driving voltage or impurities in the bilayer graphene [40]. The bilayer graphene has the shoulder-like band structure and two singularities near the zero momentum [Fig. 5(d)]. This singularity has the similar properties as the Dirac point, which plays an important role in the modulation process [40]. Calculation results in Fig. 5(c) predict that the transimissivity will have two valleys near two singularities [see Supplemental Material [33], section 5].

In summary, we achieved visible range SPP modulation through the strong light field and electric field dual-enhancement at the interface of Ag NW and the graphene sheet. The device we fabricated can operate as a 3 dB SPP modulator with a 40-μm-length silver NW. Moreover, the investigation of the modulation behavior provides further understanding of the properties of graphene in the vicinity of the Dirac point and singularity, which may suggest the possibility to

realize electrically controlled electron-phonon coupling in graphene [41]. As the SPP mode area can be further squeezed, our device may provide a way of fabricating ultra-compact nanophotonic devices and may find its applications in integrated optical circuits, nanoscaled laser sources, and optical communications etc. Besides, our device has the potential for dynamic operation and the bandwidth could approach gigahertz when the capacitance of the device is smaller than 0.1 pF.

This work is supported by National Natural Science Foundation of China (No. 61177062 and 51372220), National Key Basic Research Program of China (No. 2013CB328703), the Fundamental Research Funds for the Central Universities, the Program for Zhejiang Leading Team of S&T Innovation and the Fundamental Research Funds for the Central Universities, MANA, International Center for Materials Nanoarchitectonics, National Institute for Materials Science, Japan, and a joint project with Sungkyunkwan University, Korea. The authors thank Prof. Xiang Zhang, Prof. Shiyou Yang, Dr. Yu Ye in Berkeley, Junhao He, Pan Wang, Weisong Yang in ZJU for helpful discussions.

References

[1] J. A. Schuller, E. S. Barnard, W. Cai, Y. C. Jun, J. S. White, and M. L. Brongersma, Nature Mater. **9**, 193 (2010).

[2] W. L. Barnes, A. Dereux, and T. W. Ebbesen, Nature **424**, 824 (2003).

[3] V. J. Sorger and X. Zhang, Science **333**, 709 (2011).

[4] J. K. Kitur, V. A. Podolskiy, and M. A. Noginov, Phys. Rev. Lett. **106**, 183903 (2011).

[5] M. W. Knight, H. Sobhani, P. Nordlander, and N. J. Halas, Science **332**, 702 (2011).

[6] A. Al ù and N. Engheta, Phys. Rev. Lett. **101**, 043901 (2008).

[7] T. Sannomiya, H. Dermutz, C. Hafner, J. Vörös, and A. B. Dahlin, Langmuir **26**, 7619 (2010).

[8] S. Zhang, and H. Xu, ACS Nano **6**, 8128 (2012).

[9] R. H. Ritchie, Phys. Rev. **106**, 874 (1957).

[10] Z. L. Wang, Micron **27**, 265 (1996).

[11] J. A. Scholl, A. L. Koh, and J. A. Dionne, Nature **483**, 421 (2012).

[12] P. R. West, S. Ishii, G. V. Naik, N. K. Emani, W. M. Shalaev, and A. Boltasseva, Laser Photonics Rev. **4**, 795 (2010).

[13] F. H. L. Koppens, D. E. Chang, and F. J. García de Abajo, Nano. Lett. **11**, 3370 (2011).

[14] A. H. C. Neto, F. Guinea, N. M. R. Peres, K. S. Novoselov, and A. K. Geim, Rev. Mod. Phys. **81**, 109 (2009).

[15] A. K. Geim, Science **324**, 1530 (2009).

[16] M. V. Fistul and K. B. Efetov, Phys. Rev. Lett. **98**, 256803 (2007).

[17] T. Ohta, A. Bostwick, T. Seyller, K. Horn, and E. Rotenberg, Science **313**, 951 (2006).

[18] F. Wang, Y. Zhang, C. Tian, C. Girit, A. Zettl, M. Crommie, and Y. R. Shen, Science **320**, 206 (2008).

[19] M. Liu, X. Yin, E. U.-Avila, B. Geng, T. Zentgraf, L. Ju, F. Wang, and X. Zhang, Nature **474**, 64 (2011).

[20] B. S. Rodriguez, R. Yan, M. M. Kelly, T. Fang, K. Tahy, W. S. Hwang, D. Jena, L. Liu, and H. G. Xing, Nature Commun. **3**, 780 (2012).

[21] J. Chen, M. Badioli, P. A. -González, S. Thongrattanasiri, F. Huth, J. Osmond, M. Spasenović, A. Centeno, A. Pesquera, P. Godignon, A. Z. Elorza, N. Camara, F. J. García de Abajo, R. Hillenbrand, and F. H. L. Koppens, Nature **487**, 77 (2012).

[22] Z. Fei, A. S. Rodin, G. O. Andreev, W. Bao, A. S. McLeod, M. Wagner, L. M. Zhang, Z. Zhao, M. Thiemens, G. Dominguez, M. M. Fogler, A. H. C. Neto, C. N. Lau, F. Keilmann, and D. N. Basov, Nature **487**, 82 (2012).

[23] J. Kim, H. Son, D. J. Cho, B. Geng, W. Regan, S. Shi, K. Kim, A. Zettl, Y.-R. Shen, and F. Wang, Nano Lett. **12**, 5598 (2012).

[24] Y. Yao, M. A. Kats, P. Genevet, N. Yu, Y. Song, J. Kong, and F. Capasso, Nano Lett. **13**, 1257 (2013).

[25] Y. Xiao, Y. Francescato, V. Giannini, M. Rahmani, T. R. Roschuk, A. M. Gilbertson, Y. Sonnefraud, C. Mattevi, M. Hong, L. F. Cohen, and S. A. Maier, Phys. Chem. Chem. Phys. **15**, 5395 (2013).

[26] V. V. Temnov, G. Armelles, U. Woggon, D. Guzatov, A. Cebollada, A. G.-Martin, J.-Miguel G.-Martin, T. Thomay, A. Leitenstorfer, and R. Bratschitsch, Nat. Photonics 4, 107 (2010).

[27] M. J. Dicken, L. A. Sweatlock, D. Pacifici, H. J. Lezec, K. Bhattacharya, and H. A. Atwater, Nano Lett. **8**, 4048 (2008).

[28] B. J. Kim, H. Jang, S.-K. Lee, B. H. Hong, J.-H. Ahn, and J. H. Cho, Nano Lett. **10**, 3464 (2010).

[29] Z. Fang, S. Thongrattanasiri, A. Schlather, Z. Liu, L. Ma, Y. Wang, P. M. Ajayan, P. Nordlander, N. J. Halas, and F. J. G. de Abajo, ACS Nano **7**, 2388 (2013).

[30] K. S. Novoselov, A. K. Geim, S. V. Morozov, D. Jiang, Y. Zhang, S. V. Dubonos, I. V. Grigorieva, and A. A. Firsov, Science **306**, 666 (2004).

[31] S. Ryu, L. Liu, S. Berciaud, Y. -J. Yu, H. Liu, P. Kim, G. W. Flynn, and L. E. Brus, Nano Lett. **10**, 4944 (2010).

[32] G. Giovannetti, P. A. Khomyakov, G. Brocks, V. M. Karpan, J. van den Brink, and P. J. Kelly, Doping Graphene with Metal Contacts. Phys. Rev. Lett. **101**, 026803 (2008).

[33] See Supplemental Material at for details.

[34] A. C. Ferrari, J. C. Meyer, V. Scardaci, C. Casiraghi, M. Lazzeri, F. Mauri, S. Piscanec, D.Jiang, K. S. Novoselov, S. Roth, and A. K. Geim, Phys. Rev. Lett. **97**, 187401 (2006).

[35] L. M. Malard, M. A. Pimenta, G. Dresselhaus, and M. S. Dresselhaus, Phys. Rep. **473**, 51 (2009).

[36] T. Stauber, N. M. R. Peres, and A. K. Geim, Phys. Rev. B **78**, 085432 (2008).

[37] K. F. Mak, M. Y. Sfeir, Y. Wu, C. H. Lui, J. A. Misewich, and T. F. Heinz, Phys. Rev. Lett. **101**, 196405 (2008).

[38] R. R. Nair, P. Blake, A. N. Grigorenko, K. S. Novoselov, T. J. Booth, T. Stauber, N. M. R. Peres, and A. K. Geim, Science **320**, 1308 (2008).

[39] K. F. Mak, L. Ju, F. Wang, and T. F. Heinz, Solid State Commun. **152**, 1341 (2012).

[40] Y. Zhang, T. -T. Tang, C. Girit, Z. Hao, M. C. Martin, A. Zettl, M. F. Crommie, Y. R. Shen, and F. Wang, Nature **459**, 820 (2009).

[41] J. L. McChesney, A. Bostwick, T. Ohta, T. Seyller, K. Horn, J. Gonz ́alez, and E. Rotenberg, Phys. Rev. Lett. **104**, 136803 (2010).

Figures

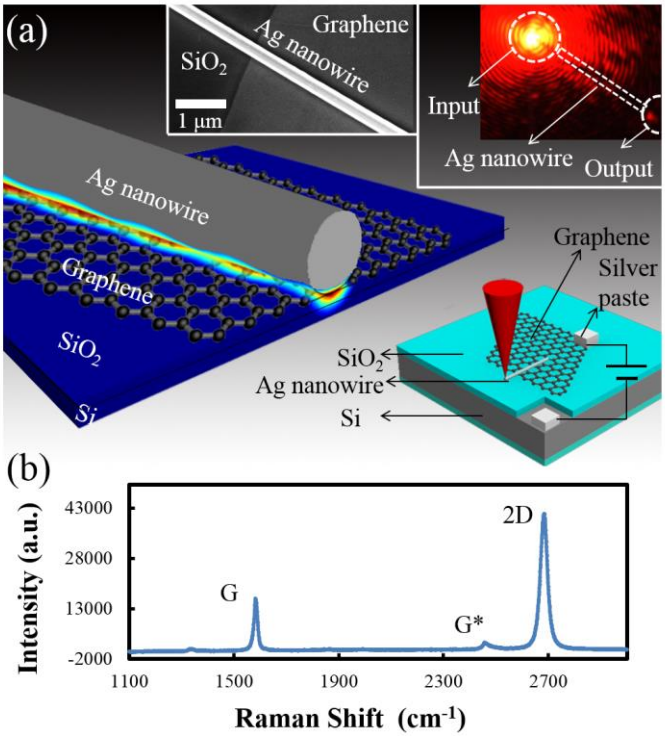

FIG. 1. (Color online). A graphene-based SPP modulator. (a) Three–dimensional (3D) schematic illustration of the device; a graphene sheet is on top of the SiO_2-Si structure. Silver paste is used as electrodes. Insets: middle, scanning electron microscopy (SEM) image of the device; upper right, an optical image of a silver NW on graphene under the excitation of a 659–nm-wavelength laser; lower right, schematic diagram of the whole structure. (b) Raman spectrum of the monolayer graphene.

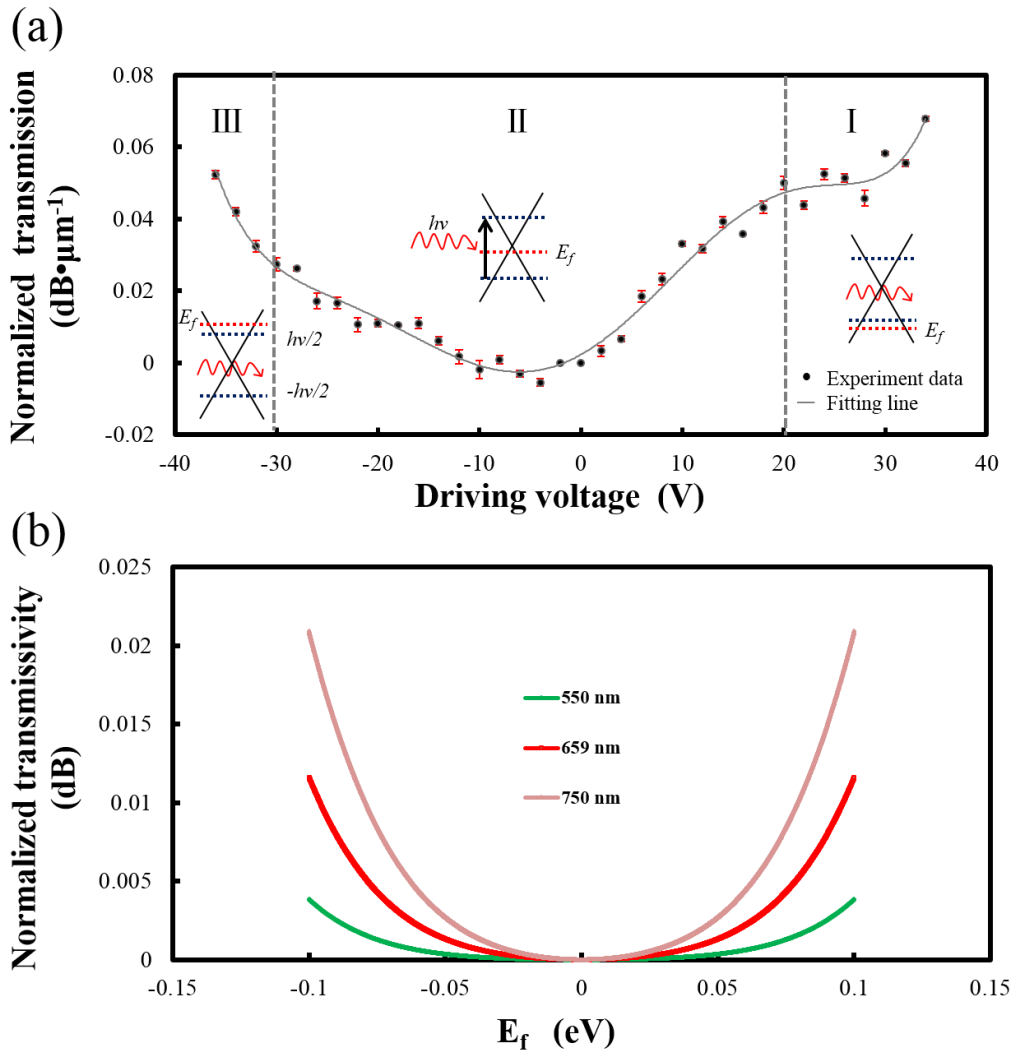

FIG. 2. (Color online). Static electro-optical response of the graphene-based SPP modulator. (a) The main panel shows the modulation depth at different driving voltages, which is normalized to the zero bias transmission (dB/μm). The grey dashed lines represent the boundary of three regions that correspond to the different injection state of the graphene sheet denoted by I, II and III. Correspondingly, the three insets show the energy band diagram of graphene in the three regions, and the arrow in the inset of region II represents the absorption of an incident photon. All of the data presented were measured for 20 times and the average value is used in the figure for accuracy and reliability. Standard deviation of the measured data is shown in Fig. S4. (b) Calculated transmissivity of single layer graphene as a function of Fermi level E_f for different wavelengths. The Fermi level can be regarded as a characterization of the driving voltage.

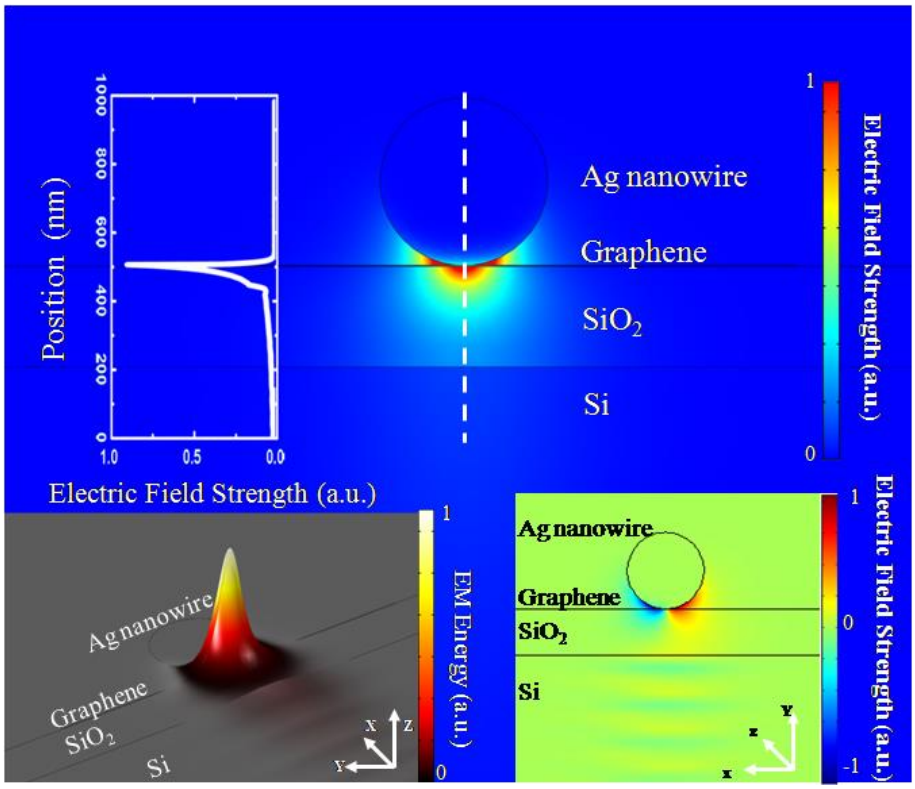

FIG. 3. (Color online). Simulated electric field distribution $(E_x^2+E_y^2+E_z^2)^{1/2}$ of the graphene-based SPP modulator using finite element method. Inset: upper left, electric field intensity at the position denoted by the white dashed line; lower left, the height-image of the electromagnetic (EM) energy distribution at the end-face of the SPP modulator; lower right, in-plane electric field distribution $(E_x^2+E_z^2)^{1/2}$ of the structure, which is very important to the interaction with the graphene sheet. A strongly confined in-plane electric field around the graphene sheet can be seen clearly.

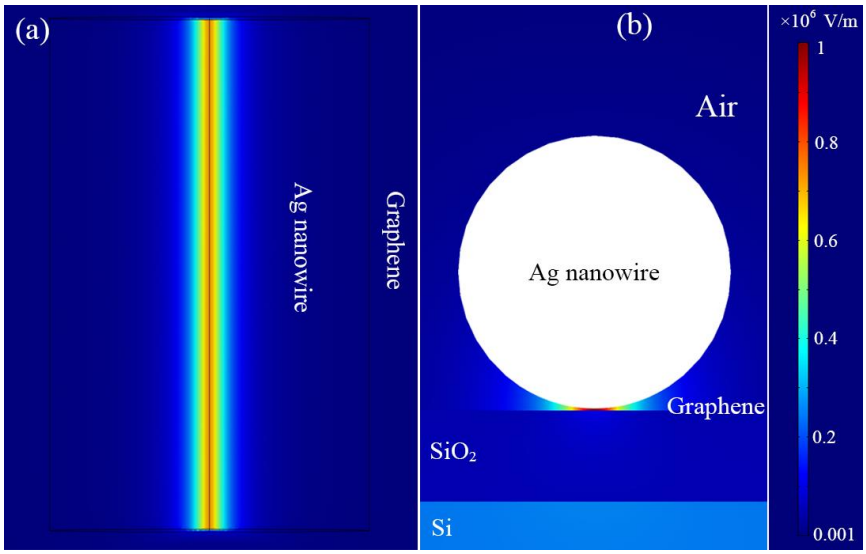

FIG. 4. (Color online). Electric field enhancement at the interface of the Ag NW and the graphene sheet. (a) Top view of simulated electric field distribution in the graphene sheet. Black lines denotes the Ag NW with 250-nm radius (b) Side view of the simulated electric field distribution of the device.

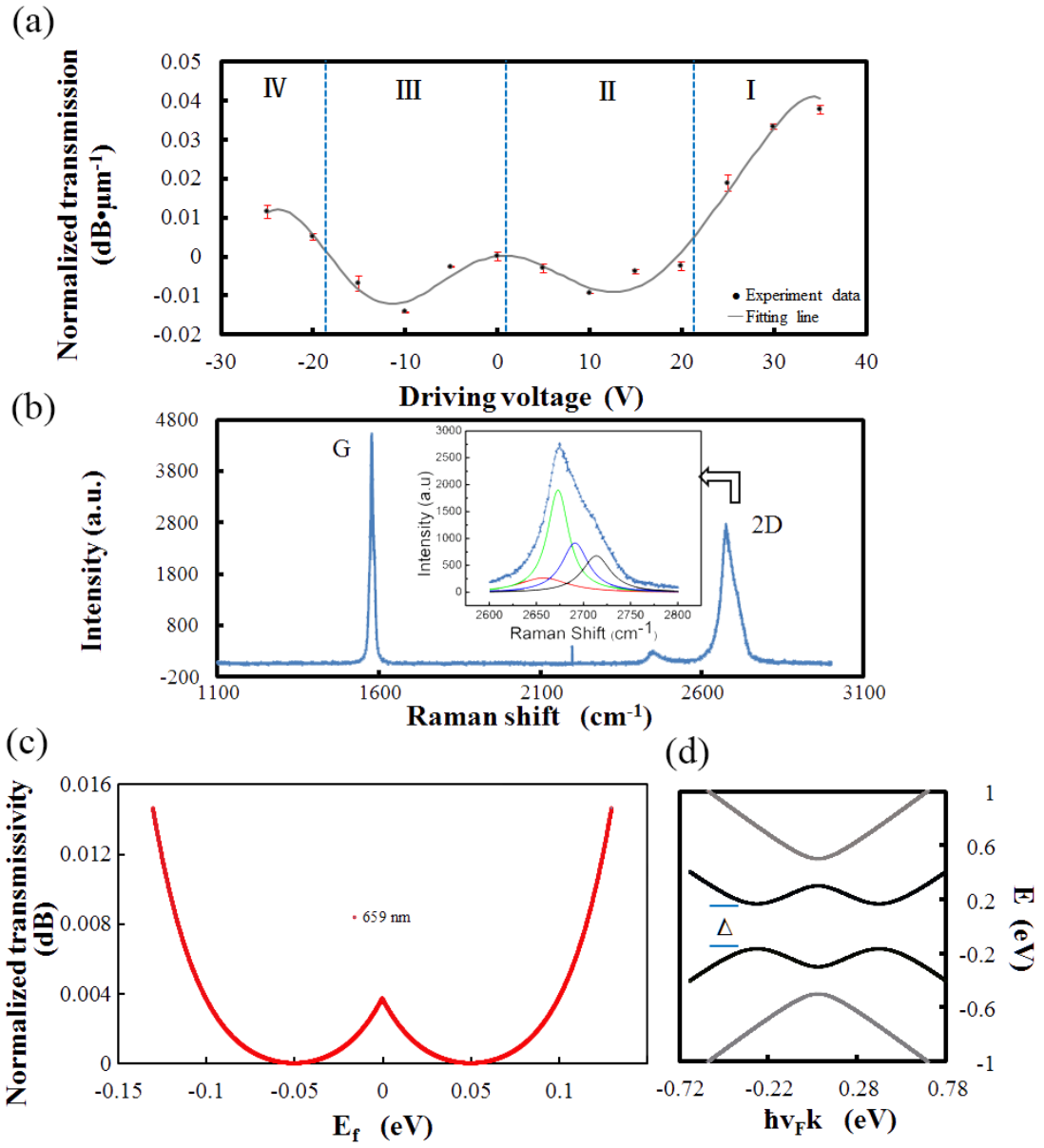

FIG. 5. (Color online). A bilayer graphene-based SPP modulator. (a) Static electro-optical response of the bilayer graphene device at different driving voltages. The data are normalized to the transmissivity with zero bias voltage. All of the data were measured for 20 times and the average value is used in the figure for accuracy and reliability. Standard deviation of the measured data is shown in Fig. S5. (b) Raman spectrum of the bilayer graphene. The inset is the 4 Lorenz curves fitting for the 2D-peak. (c) Calculated transmissivity of bilayer graphene as a function of Fermi level E_f for 659-nm-wavelengths light. (d) Band structure of the bilayer graphene in the presence of an induced gap Δ. In this calculation, Δ =0.4 eV and γ=0.4eV.